A Study of Annealing of Poly(ethylene-*co*-octene) by Temperature-Modulated and Standard Differential Scanning Calorimetry

René Androsch and Bernhard Wunderlich*

Department of Chemistry, The University of Tennessee, Knoxville, Tennessee 37996-1600, and Oak Ridge National Laboratory, Chemical and Analytical Sciences Division, Oak Ridge, Tennessee 37831-6197

Received April 8, 1999; Revised Manuscript Received July 29, 1999

ABSTRACT: Annealing of poly(ethylene-*co*-octene)s with 12−25 mass % 1-octene for 2.5−5250 min was carried out by approaching the annealing temperature through cooling at 10 K min^{-1}. Above the annealing temperature, primary crystallization was initiated. The analysis of the samples was performed during and after the annealing with temperature-modulated and standard differential scanning calorimetry, respectively (TMDSC and DSC). The irreversible annealing process consists of two different, exothermic events which are secondary crystallization and reorganization. The two processes were separated and quantitatively expressed by exponential laws with relaxation times of the order of 5 and 100 min, respectively. The two stages of crystallization and the reorganization produce a temperature-dependent, arrested, metastable, global structure of crystals and amorphous defects. Changing the annealing time can only partially compensate for changes in annealing temperature. Furthermore, TMDSC reveals a small amount of fully reversible melting. This reversible melting exists in addition to the well-known equilibrium of gauche−trans point defects in the crystal. Overall, there are thus at least five latent-heat contributions to the apparent heat capacity between the glass and melting transitions: primary and secondary crystallization, reorganization, locally reversible melting, and the gauche−trans equilibrium. For quantitative analysis of these latent-heat effects, they must be separated from the heat capacity of the melt, extrapolated from above the melting temperature, and the vibrational heat capacities of the crystal or glass.

1. Introduction

Homogeneous ethylene−1-alkene copolymers exhibit a wide variety of structures and properties which are controlled, among other parameters, by the length and structure of the branches and the comonomer concentration. In general, an increasing number of short-chain branches reduces the density and crystallinity, the melting temperature, and the crystal size and perfection. This paper focuses on the crystallization and the annealing behavior of ethylene−octene copolymers with a comonomer ratio between 12 and 25 mass % and densities ranging from 0.868 to 0.902 Mg m^{-3}. Previous investigations of ethylene−octene copolymers[1−7] in this density range have shown an extremely broad melting and crystallization range which can easily cover the entire temperature range down to the glass transition temperature of the polyethylene homopolymer[8] at 237 K.

The copolymers can have different coexisting crystalline structures,[6,7,9,10] and if the number of branches is sufficiently high, the orthorhombic crystalline form cannot be detected anymore.[3,11] For samples with a density lower than 0.90 Mg m^{-3}, fringed micellar structures increasingly replace the folded-chain lamellar morphology which is otherwise typical for the homopolymer polyethylene. Eventually, the lamellar crystals completely disappear.[12]

Recent studies of the annealing behavior showed the influence of the branch content and the annealing temperature,[5] and the combined use of calorimetry and X-ray techniques allowed the correlation to changes in the crystal morphology during stepwise heating of copolymers which were quenched and slowly cooled before analysis.[13] In this paper we discuss the kinetics of the annealing process based on measurements with standard and temperature-modulated differential scanning calorimetry (DSC and TMDSC, respectively).

Annealing is a complex process which can involve destruction of small crystals and the creation of larger crystals (Ostwald ripening, recrystallization), the perfection of existing crystals, and the formation of new crystals.[14] It was the main idea and goal of this work to separate the various events of annealing by their different kinetics and degree of reversibility using an analysis of the apparent heat capacity as a function of annealing time and temperature. Since in an isothermally performed standard DSC experiment the heat flow associated with an annealing process cannot be measured with sufficient accuracy, the heat-flow rate in cooling experiments after the isothermal annealing for given lengths of time was used to assess the overall kinetics of the annealing process. The recently developed TMDSC technique offers the added opportunity to quantitatively separate reversing and nonreversing apparent heat capacities using quasi-isothermal measurements, i.e., measurements carried out during the annealing by modulation about a fixed base temperature.[15]

In TMDSC, the programmed temperature is oscillating about an averaged temperature over one modulation cycle $\langle T \rangle$, which can be constant, as in quasi-isothermal measurements, or change linearly with time, as in the common TMDSC. The temperature−time profile is described by the underlying heating rate $\langle q \rangle$ (again, averaged over one modulation cycle), the type of the oscillation (usually a sinusoidal or a sawtooth-type

10.1021/ma9905223 CCC: $18.00
Published on Web 09/23/1999

modulation), the modulation amplitude A, and its period p. The modulation experiment is strongly influenced by the choices of the temperature amplitude and period, typically ranging from 0.1 K to several kelvins and from 10 s to several hundred seconds, respectively. The sample, therefore, is probed by two different, simultaneously applied heating rates (underlying and oscillating), and the resulting heat-flow rate, HF(t), is a superposition of the different thermal responses of the sample due to the temperature change, $T(t)$, consisting of modulation and underlying, linear change $\langle q \rangle t$. The deconvolution of the heat-flow rate into its different components by a Fourier transformation gives the unique opportunity to separate different thermal events in the sample.[16−19] In this study, most of the experiments are performed quasi-isothermally with $\langle q \rangle = 0$. The amplitudes of the first harmonic of the Fourier transform of the heat-flow rate, A_{HF}, and sample temperature, A_{Ts}, are used to calculate the reversing, apparent heat capacity C_p^{rev}. It is customary to use the term "reversing," since true reversibility must be established by thermodynamic reasoning, as is illustrated in the discussion below. The heat capacity is called "apparent" since it must be established first that latent-heat effects do not invalidate the true heat capacity:

$$C_p^{rev} = \frac{A_{HF}}{\omega A_{T_s}} K(\omega); \quad K(\omega) = \sqrt{1 + \tau^2 \omega^2} \qquad (1)$$

where $K(\omega)$ is a frequency-dependent correction factor which considers the different equilibration behaviors of sample and reference calorimeters via a time constant τ and must be determined at the given experimental conditions by measurements with different frequencies ω.[20,21] Although the abbreviated Fourier transformation filters certain thermal events from the original data, the reversing, apparent heat capacity may still contain latent-heat contributions. For samples that do not show any irreversible and reversible latent heats, C_p^{rev} is the true heat capacity of the sample. The existence of reversible latent heats can only be calculated by subtraction of the true heat capacity of the sample that must be independently known. If the reversing heat-flow rate varies with time, the process has one or more nonreversible components that need to be separated from the reversible component by studying its time dependence. It is important to note at this point that the term reversing denotes all contributions to the first harmonic term of the Fourier transform, regardless of their kinetics and degree of reversibility. Therefore, the reversing component of the modulated data, unfortunately, may contain kinetic (nonreversible) and reversible contributions.

Reversibility of crystallization and melting or, more general, of structural changes is the response to changes in equilibria, which in the case of thermal analysis, are triggered by temperature changes. Since any thermally activated transition from the melt to the crystal, and vice versa, can be reversed, the term "reversibility" needs to be defined with respect to the absolute value of the externally changed parameter, i.e., in this case the temperature amplitude. If the modulation amplitude is, for example, 20 K, a typical macroscopic melt/crystal transition in a polymer will be reversing, despite the inherent irreversibility of polymer crystallization due to crystal and molecular nucleation.[14] Considerably smaller amplitudes can cover the crystallization and melting ranges for oligomers or metals, and in the presence of crystal nuclei, sufficiently small molecules exhibit true crystallization/melting equilibria.[22] Previous investigations on poly(ethylene terephthalate)[23] and poly(oxyethylene)[24] have shown, however, that at small modulation amplitudes a small amount of reversing heat flow exists beyond that caused by the heat capacity, even for macromolecules. Furthermore, the analysis of the melting behavior of crystals that have different internal order and, therefore, melting temperatures indicates a dependence of the amount of reversible transition on the crystal quality. The poorer the crystal, the higher is the amount of the reversing transition within the applied amplitude. A special investigation could prove that the observed reversing contribution during melting is not caused by instrument effects, nor by the presence of the modulation itself.[25]

Table 1. Comonomer Content, Density, and Melt Flow Index (MFI) of the Investigated Samples

sample	comonomer content[26,27] [mass %]	comonomer content[28] [mass %]	density [Mg m^{-3}]	MFI 463 K/2.16 kp [g/10 min]
1	25	38.4	0.868	0.5
2	24	34.5	0.87	5
3	20	29.7	0.88	18
4	14	20.9	0.895	1.6
5	12	14.2	0.902	1

2. Experimental Section

2.1. Materials. The materials investigated were commercially available poly(ethylene-*co*-octene)s provided by DuPont-Dow Elastomers[26] and Dow Chemical Company,[27] respectively. The branch concentrations were determined by NMR to be between 14.2 and 38.4 mass %[28] but differ from the values given in the data sheets of the provider. This is probably caused by the also present long-chain branches which improve the processability[28−30] and control the melt flow index. The densities of the different copolymers at room temperature range from 0.868 to 0.902 Mg m^{-3}. Relevant structural parameters are summarized in Table 1[26−28] and are additionally described elsewhere[6] for the sample with a density of 0.870 Mg m^{-3}. Samples were received as cast film of a thickness of 0.1 mm or as pellets which were melt-pressed at 393 K to films.

2.2. Instrumentation. Measurements were performed on a DSC 7 and a PYRIS 1 DSC, both from Perkin-Elmer. The sample temperature was calibrated using the onset of melting of indium (429.8 K) and cyclohexane (279.6 K) on heating with a rate of 10 K min^{-1}. The heat-flow rate was calibrated with the heat of fusion of indium (28.45 J g^{-1}). Heat capacities in the standard DSC mode were obtained by the three-curve method; i.e., the heat-flow rate was baseline corrected and point-by-point calibrated with sapphire.[31] In the temperature-modulated mode, the calculation of the reversing heat capacity was done by Fourier transformation of the heating rate and heat-flow rate (see for example ref 18) and afterward frequency corrected.[20] The heating and cooling rates in standard DSC experiments were 10 K min^{-1}. The TMDSC experiments were performed quasi-isothermally with a sawtooth modulation of the program temperature using different amplitudes and frequencies. The furnace of the DSC 7 was purged with dry nitrogen and that of the PYRIS system with helium, both at flow rates of 20 mL min^{-1}. The DSC 7 was operating with an intracooler as cooling device, whereas the liquid nitrogen accessory was used in the case of the PYRIS system.

3. Results and Initial Discussion

3.1. General Description of Crystallization and Melting of Unannealed Samples by Standard DSC. Figure 1a shows cooling scans and Figure 1b heating scans of the five different poly(ethylene-*co*-octene)s as

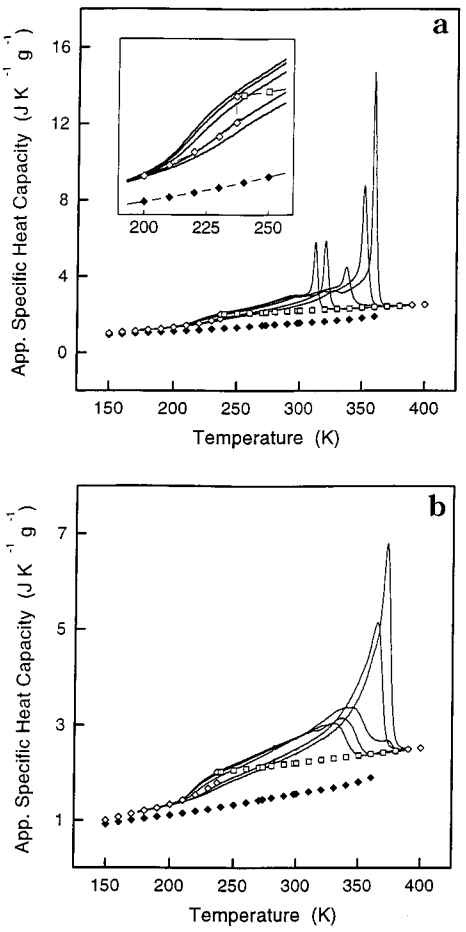

Figure 1. Standard DSC scans of poly(ethylene-*co*-octene)s with different densities, as listed in Table 1 (samples 1−5 have crystallization and melting peaks in sequence left to right): (a) cooling traces, (b) heating traces.

measured by standard DSC. The raw heat-flow data are converted into apparent heat capacities which can be compared to the true specific heat capacity obtained from the ATHAS data bank[32] (□ and ◇ for amorphous polyethylene in the liquid and glassy states, respectively; ◆ for crystalline polyethylene). The heating scans were performed immediately after the cooling scans to avoid extraneous thermal history effects as much as possible.

The cooling scans reveal clearly (1) a sharp onset of the primary crystallization process, (2) a higher apparent specific heat capacity than the true specific heat capacity until the glass transition is reached (see the insert), and (3) an increase of the total heat of crystallization with decreasing comonomer content, as listed in Table 1. The crystallization temperatures and crystallinities obtained from the cooling experiments are summarized in Table 2. To compare the samples, the crystallization temperatures are expressed by their onset temperatures. They increase with decreasing comonomer content. The apparent specific heat capacity increases with comonomer content. This is seen best immediately above the glass transition temperature, as displayed in the enlarged part of Figure 1a. The upward shift of the apparent specific heat capacity with decreasing density exceeds the expected increase of the true specific heat capacity of the sample with decreasing crystallinity. The enthalpy-based crystallinity is given in Table 2 for two different temperatures: at 293 and 233 K. The latter is close to the glass transition

Table 2. Crystallization Temperature and Crystallinity Based on Data Shown in Figure 1a

sample	crystallization temperature[a] [K]	crystallinity[b] at 293 K [%]	crystallinity[b] at 233 K [%]
1	319	13	27
2	325	15	29
3	344	23	31
4	359	37	47
5	364	42	49

[a] Onset of the crystallization on cooling at 10 K min^{-1} as seen in Figure 1a. [b] Based on a heat of fusion of 4.11 kJ (mol of CH_2)$^{-1}$ and its temperature dependence, as given in the ATHAS data bank.[32] Data from Figure 1a.

temperature, where the crystallinity reaches its final value. The crystallinity was calculated by taking into account the changes of the true specific heat capacity and the heat of fusion with temperature.[4,33,34] The crystallinity is, however, only to be used for comparison between the samples. It does not allow an absolute comparison with the homopolymer since we could show earlier that the heat of fusion in these copolymers is probably lower than the 4.11 kJ (mol of CH_2)$^{-1}$ known for polyethylene, and further complications arise from the existence of different crystalline phases in the samples, identified by X-ray diffraction.[9,10]

The observations from Figure 1 suggest that there is a latent-heat effect over the entire temperature range between the onset of crystallization and the glass transition temperature, causing an apparent specific heat capacity above the upper limit of the specific heat capacity of the amorphous polyethylene in the liquid state (open symbols). This is particularly true for the samples with a density equal to and lower than 0.88 Mg m^{-3}; i.e., exothermic processes continue down to the glass transition temperature. The crystallization consists, thus, of at least two different processes which show up as the sharp transition of the primary crystallization at high temperature and a broad transition at lower temperature. These two processes must have different kinetics, as was already suggested and proven in an earlier work on poly(ethylene-*co*-octene) with a density of 0.870 Mg m^{-3}.[6]

The heating scans in Figure 1b are characterized by trends in the shape, peak, and end of melting temperatures, the apparent specific heat capacities, and the heats of transition. All of these go parallel to the cooling scans, except that the melting peaks are considerably broader than the crystallization peaks and occur at higher temperature than the crystallizations. As usual, the glass transition broadens with increasing crystallinity to higher temperature, and in all cases melting starts without break, contiguous with the glass transition temperature, and is finished at a higher temperature for samples with higher room-temperature density.

The melting and crystallization behavior of the ethylene−octene copolymers in the density range which is of interest to this work is well-known from earlier investigations performed on similar copolymers.[1−5,13] Here, we need to point out the shapes of the cooling curves which reveal a distinct heterogeneous transition behavior. Mathot et al.[1−3] discussed the shape of the DSC curves in terms of intermolecular and intramolecular homogeneity of the distribution of the short-chain branches (SCB) but refer mainly to the heating scans, not the cooling scans. The reason for differently shaped heating and cooling scans can be explained by the differences in melting and crystallization mecha-

nisms. Crystallization needs crystal and molecular nucleation, causing a large supercooling.[14] Melting, in contrast to crystallization, shows for small crystals practically no superheating; i.e., it requires a much smaller activation energy than crystallization and is also not kinetically hindered by diffusion processes.[35] Crystallization and melting curves must thus be different in shape. This includes also copolymers that have homogeneously incorporated SCBs. The heating scans (Figure 1b), indeed, show no distinct peak like the cooling scans, but closer inspection of the high end of the melting process reveals a reproducible shoulder/peak which probably accounts for the initial crystallization process. This does not necessarily mean that the branches are heterogeneously distributed in the main chain but are caused by different nucleation/growth mechanisms for different types of crystals growing during cooling. Although some intermolecular heterogeneity has been proven earlier by multiple-step isothermal crystallization experiments in some other commercially available metallocene-catalyzed polyethylene copolymers,[36] the visual differences between cooling and heating scans can be explained sufficiently without any assumptions about the incorporation of branches into the crystals. In fact, we are not aware of any chemical heterogeneties in our samples and have no reason to discuss our results in such terms.

From a comparison of heat capacities of various polyethylenes, it is known for some time that samples of lower crystallinity are within their melting range at ambient temperature.[37] It must, thus, be assumed, and will be discussed later in this paper, that polymers can reach temperature-dependent, metastable, local equilibria in their melting range.

3.2. Annealing Behavior, Measured by Standard DSC. The annealing behavior of two of the copolymers is displayed in Figure 2. Cooling scans by standard DSC of sample 2 with a density of 0.870 Mg m^{-3} (a) and sample 5 with a density of 0.902 Mg m^{-3} (b) are shown after annealing for different times at 299 K. The shortest and longest annealing times were chosen to be 2.5 and approximately 5000 min, respectively. The heat-flow rate for annealing times of less than 2.5 min results in erroneous data reduction for the subsequent cooling scan, and after approximately 5000 min the annealing process is slowed sufficiently to yield little additional information, as will be discussed below.

When the sample is kept at the annealing temperature for increasing lengths of time, the heat-flow rate on further cooling does not immediately approach the value of the continuously cooled sample (0 min annealing). This level of the continuously cooled sample is reached at increasingly lower temperatures with annealing time. This is best seen for the sample shown in Figure 2a, which was annealed for 5260 min. The heat-flow rate reaches its steady-state value at approximately −3.36 mW and not the value of −4.16 mW, which was measured for the unannealed sample at 295.5 K. The difference in the heat-flow rate corresponds to a decrease in the apparent specific heat capacity of 0.5 J K^{-1} g^{-1}. Similar data for this particular sample were also taken at annealing temperatures of 313 and 283 K. All other copolymers were annealed at 299 K only. The sample with the higher density of 0.902 Mg m^{-3} (Figure 2b) shows similar effects, but not as distinct as observed in the samples with a density equal to and lower than 0.88 Mg m^{-3}.

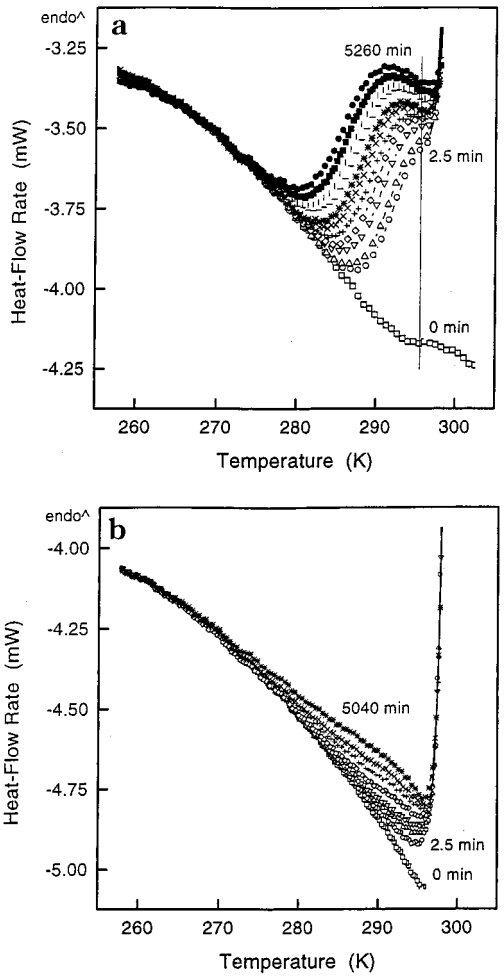

Figure 2. Standard DSC cooling scans of poly(ethylene-*co*-octene)s after annealing for different times at 299 K: (a) density 0.870 Mg m^{-3}, sample 2; (b) density 0.902 Mg m^{-3}, sample 5.

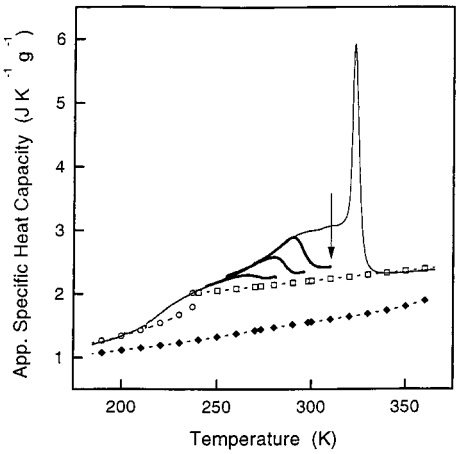

Figure 3. Standard DSC cooling scans of poly(ethylene-*co*-octene) (density 0.870 Mg m^{-3}, sample 2). From right to left: continuous cooling (thin line), after annealing for approximately 5000 min at 313, 299, and 283 K (bold lines, the arrow marks the 313 K annealing temperature).

The decrease of the apparent specific heat capacity of sample 2, annealed for the longest time at each of the three annealing temperatures is illustrated in Figure 3, where it is compared to the apparent specific heat capacity of the unannealed sample. It can clearly be seen that the annealing process reduces the apparent specific heat capacity considerably but does not even

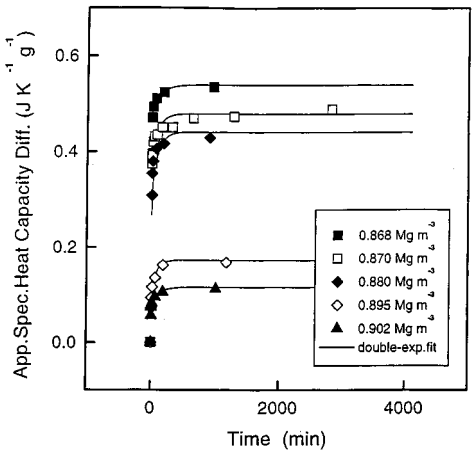

Figure 4. Difference between the apparent specific heat capacity of the unannealed sample and annealed samples 1−5 (top to bottom) as a function of annealing time at 299 K.

reach the value of the true specific heat capacity of the liquid (open squares) which is the upper limit of the specific heat capacity of the sample since the specific heat capacity of the crystalline phase is even lower (filled diamonds). At the annealing temperature, the material is already in a semicrystalline state, and the true specific heat capacity should be located between the limiting values of the crystalline and amorphous phases. After annealing, therefore, the obtained heat-flow rates still have a latent-heat component which points to a local, reversible equilibrium of crystallization and melting. The metastable system reaches a different level of perfection for each annealing experiment. A decrease in temperature, even if small, results in a new, higher ordered structure which is easily characterized by the heat flow observed on further cooling. Similarly, when the temperature is increased, the system reaches practically instantaneously the new metastable equilibrium characteristic for the higher temperature.

It cannot be assumed that annealing beyond the chosen 5000 min will result in an even lower value of the heat-flow rate on further cooling since the rate of the annealing process practically has reached zero. The time dependence of the annealing process has been monitored by the difference between the apparent heat capacities of the unannealed and annealed samples, plotted versus the annealing time t as is shown in Figure 4:

$$\Delta c_p(t) = c_p(t_0) - c_p(t) \qquad (2)$$

It can clearly be seen that $\Delta c_p(t)$ increases with decreasing density of the sample and with time. After 500−1000 min the changes become small, and a further decrease of the apparent specific heat capacity is not expected. The density, which is proportional to branch content and crystallinity, results in remarkable differences in the absolute values of Δc_p, as can also be seen in Figure 4.

The reduction of the apparent specific heat capacity with time is a direct measure of the transformation of amorphous, liquidlike material into the crystalline phase and/or an improvement of the quality of the crystalline phase. The two processes cannot be distinguished by standard DSC. To obtain some quantitative information about the approach to the metastable equilibrium, the data of Figure 4 were fitted to an expression with two relaxation times τ_1 and τ_2:

$$\Delta c_p(t) = \Delta c_p(\infty) + a_1 e^{-t/\tau_1} + a_2 e^{-t/\tau_2} \qquad (3)$$

where $\Delta c_p(\infty)$ is the fitted difference between the apparent heat capacities of the annealed and unannealed sample in metastable equilibrium after long annealing times, and a_1 and a_2 are the corresponding amplitudes of the exponential decays. The importance of this data treatment is the proof of the existence of two relaxation processes. The fast event in the beginning of the annealing process has a time constant of about 5 min and is independent of the branch content or, at least, does not systematically change. The second process takes 10−50 times longer; i.e., the time constant τ_2 is on the order of 100 min. Naturally, the fitting procedure contains considerable errors due to the small number of data points, which, in addition, are rather difficult to determine at short annealing times, but each attempt to use a single-exponential approach to the equilibrium value failed to give any reasonable fit, and the obtained time constants τ_1 and τ_2 are reproducible in their approximate ratios, i.e., 2−5 min vs 78−137 min. It will be shown below how more reliable kinetic constants can be measured, albeit the fact of the existence of two time constants and their approximate ratio is already established by the standard DSC data shown in Figure 4. The differences between the apparent heat capacities of the annealed and unannealed sample, $\Delta c_p(\infty)$, give an almost linear relation, when correlated to the comonomer content given in column 2 of Table 1. This can be taken as proof that structural changes during annealing are more likely in samples with a higher comonomer content, which, in turn, cause a more restricted main crystallization; i.e., branches slow down the crystallization and lead to poorer crystals during the primary crystallization.

On further cooling, the heat-flow rate and apparent specific heat capacity remain at an approximately constant level for up to 10 K for the samples with a density equal to and lower than 0.88 Mg m^{-3}. The width of this temperature range depends on the annealing time. Thereafter, the rate of heat flow and the apparent specific heat capacity change sharply back to the level of the unannealed sample. The approach to the heat-flow rate of the unannealed sample is more gradual for the two samples of higher density (compare parts a and b of Figure 2). The differences between the heat-flow-rate curves of the unannealed and annealed samples are proportional to the total energies released in the annealing process. As stated earlier, the annealing process consists of two different events which do not allow to assign the observed released total energy to a single, secondary crystallization process; it could also be a superposition of crystallization and reorganization. The sharp return to the level of the unannealed sample indicates that longer annealing times cannot compensate the shift in metastable equilibrium that seems to apply at lower temperatures; i.e., the arrested global structure is temperature-dependent.

After annealing, the cooling scans shown in Figures 2 and 3 were continued to 253 K, except for the annealing at 283 K which was continued to 233 K. These samples were then immediately reheated to assess the crystallinity by DSC on melting. The heating scans, obtained on the same samples as shown in Figure 2a,b, are reproduced in Figure 5a,b. Annealing results in the

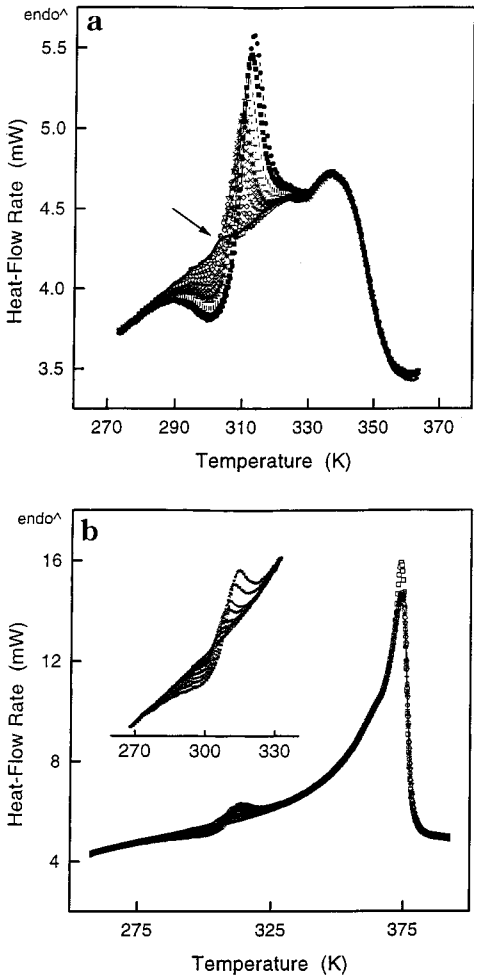

Figure 5. Standard DSC heating scans of poly(ethylene-*co*-octene) after annealing for different times at 299 K and cooling to 253 K: (a) density 0.870 Mg m^{-3}, sample 2; (b) density 0.902 Mg m^{-3}, sample 5. Symbols as in Figure 2.

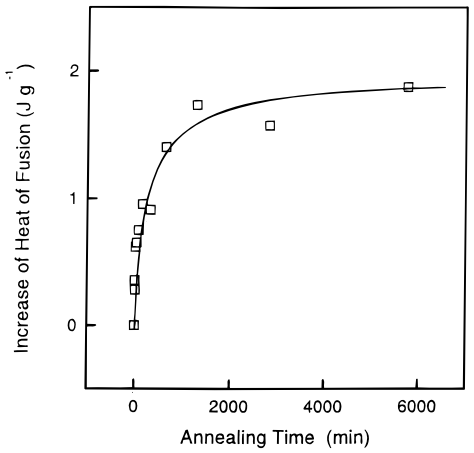

Figure 6. Difference of the total heat of fusion between the annealed and unannealed samples as a function of the annealing time for poly(ethylene-*co*-octene) analyzed in Figure 5a (density 0.870 Mg m^{-3}, sample 2).

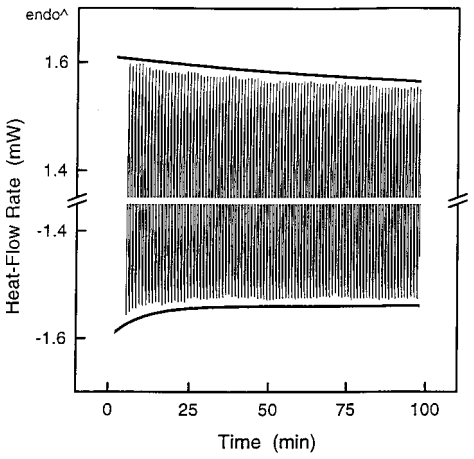

Figure 7. Modulated heat-flow rate of poly(ethylene-*co*-octene) (density 0.870 Mg m^{-3}, sample 2) as a function of time at 299 K (amplitude 1.0 K, period 60 s).

appearance of a distinct minimum in the heat-flow rate in the vicinity of the annealing temperature, followed by a maximum at slightly higher temperature. The minimum in the heat-flow rate is interpreted as a missing heat of melting, when compared to the heat-flow rate of the sample with zero annealing time. Obviously, the perfection of the crystals melting in this temperature range in the unannealed sample has been changed in the annealing process. It is straightforward to assume that the improved crystals melt at a higher temperature which causes the new maximum in the heat-flow-rate curves in Figure 5. An increase in the total heat of fusion vs annealing time shows the same dependence on annealing time as the apparent specific heat capacity difference of Figure 4.

The increase of the total heat of fusion with annealing time, displayed in Figure 6, was calculated as difference of the integrated apparent specific heat capacity between the annealed and unannealed samples, covering both the minimum and the maximum in the heat-flow rate:

$$\Delta h_f(t) = \int_{273\ \mathrm{K}}^{333\ \mathrm{K}} [c_p(t)](T)\ \mathrm{d}T - \int_{273\ \mathrm{K}}^{333\ \mathrm{K}} [c_p(t_0)](T)\ \mathrm{d}T \quad (4)$$

In the beginning of the annealing process there is a larger increase of the total heat of fusion, and after 500−1000 min the further increase is negligible. An interpretation of the absolute increase of the heat of fusion in terms of crystallinity is somewhat difficult since the heat of fusion increases also when the internal order of the crystals improves, and not only by an increase in amount of crystals. The maximum increase in crystallinity of the shown examples lies within the range of 1−5%. Similar to the cooling experiment after the annealing process, further conclusions about the nature of the structural changes within the sample cannot be drawn from the DSC heating data.

There is, however, an indication that some new crystals do form in the beginning of the annealing process. After 1 min of annealing, a small melting peak appears that is not compensated by a corresponding minimum in $c_p(t)$ in Figure 5a. The maximum in the bold line of Figure 5a is marked by an arrow. The minima partially compensating for the corresponding melting peaks can be detected only at longer annealing times.

3.3. Annealing Behavior, Measured by Temperature-Modulated DSC (TMDSC). Figure 7 shows typical raw data of the modulated heat-flow rate in the time domain for a quasi-isothermal annealing at 299 K measured on poly(ethylene-*co*-octene) with a density of 0.870 Mg m^{-3} (sample 2). This particular sample was cooled at 10 K min^{-1} from the melt at 393 K to the annealing temperature and then was modulated with

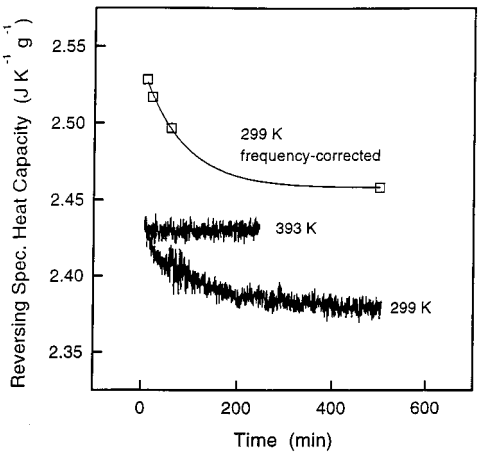

Figure 8. Reversing specific heat capacity of poly(ethylene-*co*-octene) (density 0.870 Mg m^{-3}, sample 2) as a function of time at 299 and 393 K (amplitude 1.0 K, period 60 s). Open squares are the frequency-corrected data.

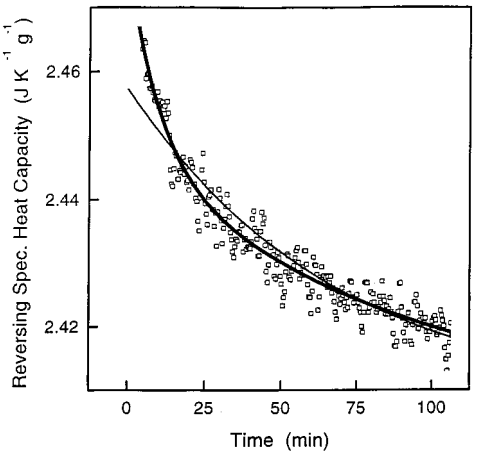

Figure 9. Fit of the reversing specific heat capacity of poly(ethylene-*co*-octene) (density 0.870 Mg m^{-3}, sample 2) as a function of time using a single and two exponential decays (amplitude 1.0 K, period 60 s).

an amplitude of 1.0 K and a period of 60 s. Because of instrumental reasons, recording of the heat-flow rate starts after three initial cycles; i.e., the first 3 min of the annealing process is not recorded in this plot. The envelopes of the minima and maxima of the heat-flow rate (slightly displaced for clarity) indicate the time dependence of the transition for each segment of heating and cooling. It can be clearly seen that the shape of the upper envelope is different from that of the lower; i.e., the time dependence of the melting kinetics is different from that of the crystallization kinetics. Both maxima and minima of the heat-flow rate are getting smaller in accordance with the time constants τ_1 and τ_2, which were already observed by the change of the apparent specific heat capacity by standard DSC in Figure 4.

The calculated reversing specific heat capacity [eq 1 with $K(\omega) = 1$] is shown in Figure 8. After approximately 5 min of annealing, it reaches 2.43 J K^{-1} g^{-1} and decreases further to 2.37 J K^{-1} g^{-1} over the course of the monitored 500 min. After 500 min, the reversing specific heat capacity becomes almost constant. The exponential decrease of the reversing specific heat capacity is entirely due to changes in the sample. All instrumental effects, which always need to be considered in this type of experiment,[15] are excluded, as is proven by the constant reversing specific heat capacity at 393 K where the same sample is in equilibrium as a melt (center curve of Figure 8). The open squares in the upper curve of Figure 8 represent the frequency-corrected data of the reversing specific heat capacity, calculated using eq 1 with $\tau \approx 3$ s, a value obtained by fitting data from experiments with periods of 40, 60, 96, and 192 s. The corrected value obtained after 500 min is ca. 2.46 J K^{-1} g^{-1}. For very long times the reversing specific heat capacity decreases further, but only to ca. 2.44 J K^{-1} g^{-1}. The reversing specific heat capacity of Figure 8 can be fitted, as expected, by the same function as is given by eq 3 which was used to describe the time dependence of the apparent specific heat capacity measured by standard DSC and is shown in Figure 4 (curve two from the top). Figure 9 finally underlines the necessity to use two exponential terms. The thinner line is an unsuccessful fit using only one time constant. It does not agree with the experiment at short times.

The quasi-isothermal TMDSC data shown in Figures 7−9 confirm the results obtained by standard DSC, discussed in the previous section. The TMDSC, however, is able to monitor the kinetics and the type of structural changes directly, without the need to perform subsequent scanning experiments. Furthermore, the annealing process can be followed continuously and not only at discrete times. The most important advantages are (1) the separation of the superimposed melting and crystallization processes and (2) the on-line measurement of the change of the reversing specific heat capacity with time. As can be seen in Figures 7−9, the reversing specific heat capacity is not constant but approaches a metastable equilibrium in a superposition of two different processes. When the reversing specific heat capacity reaches a constant value after 500−1000 min, the crystallization and melting processes within each modulation cycle are truly reversible within the temperature range of the modulation. The corrected, apparent reversing specific heat capacity of all investigated samples, however, stays well above the specific heat capacity expected for the sample at the given crystallinity. At 299 K the extrapolated, reversing specific heat capacities of the different copolymer samples 1−5 of Table 1 range from 2.27 to about 2.45 J K^{-1} g^{-1}, while the specific heat capacity of the liquid is 2.22 J K^{-1} g^{-1}. These differences in specific heat capacity are at present difficult to discuss further since the basic specific heat capacity which is free of melting and crystallization effects, as obtained from the ATHAS data bank, changes with crystallinity. Consequently, the straightforward, quantitative correlation of the amount of reversible melting to chemical structure and crystal morphology was not made.

The annealing process is irreversible and is indicated by the decreasing reversing specific heat capacity up to about 500−1000 min of the experiments. Irreversible processes, in general, are kinetically controlled, as proven by TMDSC when the experiments are performed with different frequency.[38−41] Figure 10 shows such frequency-dependent TMDSC on cooling with an underlying cooling rate of 1.0 K min^{-1} for sample 2 of Table 1. The open diamonds and squares mark the amorphous specific heat capacity of polyethylene through the glass transition region, and the filled diamonds mark the crystalline specific heat capacity of polyethylene, which at low temperatures is also a measure of the specific heat capacity exclusively due to vibrations.[32] The higher the modulation frequency, the lower is the reversing specific heat capacity in the transition range. The data

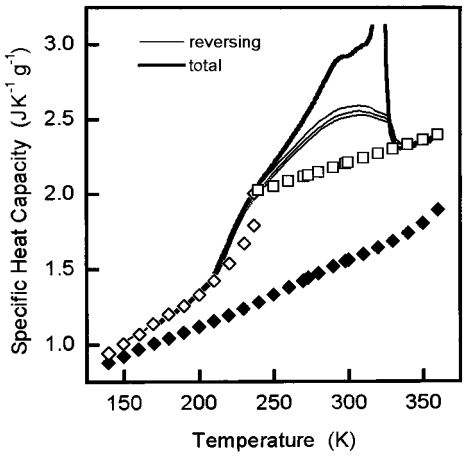

Figure 10. Reversing specific heat capacity of poly(ethylene-*co*-octene) (density 0.870 Mg m^{-3}, sample 2) by TMDSC on cooling as a function of temperature and modulation frequency. Periods of 30, 60, and 120 s and amplitudes of 1.75 K (from top to bottom, respectively). The heavy line is the total apparent specific heat capacity by standard DSC as in Figure 1a, included in the figure for comparison.

need to be compared with those of Figure 1a, which represent the total apparent specific heat capacity. As already illustrated in an earlier study,[6] the narrow exotherm in the beginning of the crystallization does not appear in the reversing specific heat capacity of Figure 10; i.e., it corresponds to a completely irreversible process. Albeit small in effect, the data in Figure 10 are indeed dependent on frequency, clearly indicating that in the entire temperature range between 333 K and the glass transition irreversible processes occur. From the more detailed analysis with the quasi-isothermal TMDSC of Figures 7−9 it is clear, however, that the frequency range in Figure 10 is insufficient to identify more than the first relaxation time τ_1.

Summarizing, the crystallization in the investigated samples consists at least of four different processes involving latent heats: (1) an irreversible, primary crystallization in the beginning of crystallization with a heat of transition that decreases with comonomer content (sharp exotherm in Figure 1a), (2, 3) an irreversible, secondary crystallization and a reorganization over the entire temperature range from the beginning of primary crystallization down to the glass transition, describable by separate relaxation times in the 5 and 100 min ranges, and (4) a reversible crystallization and melting contribution to the apparent specific heat capacity that increases with increasing temperature.

4. Final Discussion of Irreversible and Reversible Crystallization and Melting

The cooling curves of Figure 1a have been quantitatively separated by the above analyses into four processes. Most prominent is the primary, irreversible crystallization peak that leads to the common lamellar structure, also seen in the here analyzed copolymers.[42] The corresponding primary crystallization peak is absent in the reversing, apparent heat capacities of the TMDSC cooling curves of Figure 10. Quite similar is the melting behavior of well-crystallized poly(oxyethylene).[24] It shows no reversing melting contribution in quasi-isothermal TMDSC. This part of the experiments follows largely the description of crystallization and melting of flexible macomolecules based on the "chain-folding principle",[43] the "crystal and molecular nucleation",[14] and the knowledge of "supercooling and superheating".[35] The primary crystallization and the annealing and zero-entropy-production melting of the so-grown crystals is not further discussed in this paper. This primary crystallization sets up the typical semicrystalline structure that consists of nanophase separated crystals and amorphous defects.[43] Its kinetics of growth is commonly represented by an Avrami-type expression.[14] It is known, however, that the melting characteristics of the primary crystals change with crystallization time, an indication that crystal perfection occurs as soon as the initial crystals are formed.[14]

The next observation is the broad crystallization region, which extends from the initial, primary, sharp crystallization peak to the glass transition region, as seen in Figure 1a. It is driven mainly by local supercooling of mobile chain segments within the amorphous defects of the semicrystalline structure, set up by the primary crystallization. These chain segments are attached to the crystals and sufficiently short or interrupted by comonomer units that multiple folding is not likely. As the crystallization temperature decreases, one expects to generate a continuous distribution of secondary crystals which decrease in size. The more the crystallization temperature decreases, the more the new crystallites are of the "fringed-micellar" morphology and macroconformation.[43] Their presence was implied earlier by the often reported "annealing peaks" produced on DSC when heating semicrystalline samples that were heat-treated at temperatures below their melting temperatures.[35] The annealing peaks appear typically between 5 and 15 K above the temperature of heat treatment (see also Figure 5). On annealing at higher crystallization temperatures, this effect can also be identified as deviation from the Avrami equation that fits the primary crystallization kinetics.

Figure 3 illustrates that this secondary crystallization is, indeed, governed not only by its kinetics but also by the local (metastable) equilibria that are set up by the prior crystallization. If only the global supercooling from equilibrium at 414.6 K would govern the kinetics and not the local supercooling, longer annealing times at higher temperature would complete the crystallization now only seen at lower temperature. Note that the overall crystallinity of the discussed samples lies between 10 and 50%, insufficient to change the branch-content concentration in the melt to move the melting/crystallization temperature by as much as the required 175 K.

The annealing of the series of low-temperature-crystallized, secondary-crystal population shown in Figures 2 and 5 and their analyses in Figures 3−9 separate three further processes. Early in the annealing, there is an exotherm with a short relaxation time of about 5 min which overlays a reversing exotherm/endotherm with a relaxation time of about 100 min (see Figures 5a, 7, and 9) and a time-independent reversible exotherm/endotherm (shown in Figures 4 and 8). The first process is considered the continuing secondary crystallization of the sample. The second is a coupling of reorganization to the locally reversible crystallization and melting. As crystals perfect by reorganization, they or their surfaces cannot participate in the reversible melting and recrystallization. It was shown for poly(ethylene terephthalate) that the reduction in reversing amplitude with time, as seen in Figures 7−9, is not

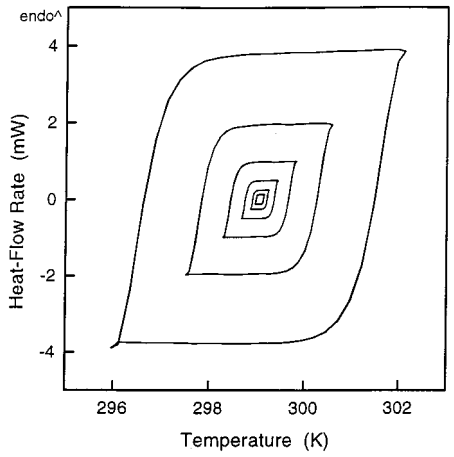

Figure 11. Lissajous figures of quasi-isothermal TMDSC at 299 K of sample 2 (density 0.870 Mg m^{-3}) after more than 5000 min of annealing, i.e., plots of heat-flow rate vs sample temperature. Period 80 s and amplitudes of 0.1, 0.2, 0.4, 0.8, 1.6, and 3.2 K.

affected by the reversing melting and crystallization itself but occurs to the same degree also without modulation.[25] The third process is a time-independent local equilibrium that is similar in appearance to the reversible melting and crystallization observed on quasi-isothermal TMDSC of nucleated indium about the melting temperature.[44]

Reversibility of crystallization and melting is a phenomenon that cannot be explained with classical theories of melting and crystallization of polymers,[14,31,35] where the phase transformation from the solid crystalline phase to the melt and vice versa is considered to be an irreversible process. Crystallization should always occur via nucleation with supercooling (i.e., the creation of the appropriate crystal and molecular nuclei), followed by crystal growth, and perfection. After crystal growth and perfection are completed, melting can only occur at a considerably higher temperature. Although crystal nucleation can be avoided by seeding with heterogeneous nuclei or incomplete melting, molecular nucleation cannot be avoided. Reducing the molecular length to that of oligomers and decreasing the crystal perfection by fast crystallization of the global crystal matrix, the temperature region of metastability of poly(oxyethylene) melt could be reduced sufficiently, so that it could be bridged by the amplitude of temperature modulation of TMDSC.[24] There remained, however, a measurable supercooling between the crystallization exotherm and the melting endotherm. Figure 11 illustrates that in the present case the heating and cooling cycles are fully reversible and independent of modulation amplitude; i.e., molecular nucleation had been eliminated. The Lissajous figures of the sawtooth modulation represent, when starting at the lower left corner, the approach to steady state which leads into the close to horizontal upper line that indicates a steady-state latent-heat contribution. The subsequent cooling cycle has no indication of supercooling.

The explanation for such reversible crystallization and melting must be that small chain segments arrested on one or both sides are involved in the process. It is known, for example, that side chains of polymers, as soon as they are tied to the main chain with a flexible spacer of four to eight CH_2 groups, can crystallize and melt similar to the corresponding small molecule, i.e., crystallize and melt reversibly with melting temperatures not far from the small molecules, severed from the main chain.[35] The analysis temperature of 299 K used in Figures 7−9, for example, could correspond to the melting points of chain segments of 20−30 chain atoms. Paraffins of this length show no supercooling, as is found in an ongoing investigation in our laboratory. Two locations offer themselves in the structure of semicrystalline polymers for such chain segments. One is found for chain segments that melt only partially because of their attachment to other, higher melting parts of the crystalline matrix; the other is found for secondary, fringed-micellar crystals, grown within the network of the primary crystals. In both cases, the amount of material and its local equilibrium melting temperature can be extracted from the here generated data.

Taking the data at 299 K listed in the discussion of Figure 8 for sample 2, the modulation of 1.0 K with the latent-heat contribution to the true heat capacity of the semicrystalline sample is about 0.28 J K^{-1} g^{-1}. (The C_p of the melt is decreased by 0.06 J K^{-1} g^{-1} for the existing 10% crystallinity.) This latent heat involves a crystallinity change of 0.28 J K^{-1} g^{-1} × 1.0 K × 14.03 g mol^{-1} × 100/4110 J mol^{-1} = 0.10%. Secondary, fringed-micellar crystals of this amount can easily be accommodated in the melting curves of the samples. Assuming, further, that all of the roughly 10% crystals of the analyzed samples show such reversible crystallization and melting on their surfaces and that these crystals are isometric with a dimension of 5.0 nm, only ca. 1.5% of a monomolecularly occupied surface layer of 0.5 nm thickness needs be involved in the reversible melting and crystallization to account for the higher apparent heat capacity. If this were one single molecular segment on each of the four growth faces of the assumed crystal, it would have a molar mass of the proper magnitude to melt and crystallize at 299 K, namely 282 Da ($\approx C_{20}H_{40}$). Both estimates show that in such a poorly crystallized sample it is possible to have local equilibria that are not restricted by molecular nucleation.[45]

This locally reversible melting and crystallization is probably a different event than the experimentally verified surface melting of lamellar structures.[46−48] The latter process was not measured with such small temperature amplitudes as usually is done in TMDSC, and a small hysteresis of the temperature dependence of the crystallinity was measured,[47] which is not indicative of the truly reversible process discussed here (see Figure 11).

A final contribution that raises the heat capacity of crystals of polyethylene above the vibrational C_p was first identified some 30 years ago[49] and is based on local point defects based on trans−gauche equilibria. It begins at about 250 K and reaches about 2% gauche concentration at the equilibrium melting temperature (414.6 K).[50]

To summarize this discussion, there are six different contributions to the apparent heat capacity in the melting and crystallization region of the analyzed polymer. The first three are truly reversible: The vibrational heat capacity, the gauche−trans equilibrium, and the reversible melting fraction. The second three are increasingly irreversible: Contribution four involves crystal perfection with a 100 min relaxation time, and contribution five is the secondary crystallization with a time constant of approximately 5 min. Both contributions four and five may contribute to the an-

nealing peak with a temperature difference between formation and melting of 5−15 K. Finally, contribution six is the primary crystallization and melting which commonly is the biggest effect and shows temperature differences between crystal growth and melting of usually 10−30 K.

This research on poly(ethylene-*co*-octene) clearly shows all six caloric effects summarized in the last paragraph. A series of homopolymers analyzed recently in our laboratory with TMDSC show that parts of the same nonreversing and reversing behavior of melting, crystallization, and annealing seem to occur universally in flexible macromolecules. The homopolymers were poly(oxyethylene),[24] poly(ethylene terephthalate),[23] poly(trimethylene terephthalate),[51] and polydioxanone.[52] We expect, thus, that the processes described in this paper have rather broad applicability to the field of polymers, and their understanding will permit a better link between structure and properties.

Acknowledgment. The authors gratefully acknowledge the calculation of the crystallinity by Dr. M. Pyda of our laboratory. The samples were graciously provided by Dr. M. Y. Keating of the DuPont Co. This work was supported by the Division of Materials Research, National Science Foundation, Polymers Program, Grant DMR-9703692, and the Division of Materials Sciences, Office of Basic Energy Sciences, U.S. Department of Energy at Oak Ridge National Laboratory, managed by Lockheed Martin Energy Research Corp. for the U.S. Department of Energy, under Contract DE-AC05-96OR22464.

References and Notes

(1) Mathot, V. B. F.; Scherrenberg, R. L.; Pijpers, T. F. J.; Engelen, Y. M. T. Structure, crystallization and morphology of homogeneous ethylene−propylene, ethylene−1-butene and ethylene−1-octene copolymers with high comonomer contents In *New Trends in Polyolefin Science and Technology*; Hosoda, S., Ed.; Research Signpost: Trivandrum, India, 1996; p 71.
(2) Mathot, V. B. F.; Scherrenberg, R. L.; Pijpers, T. F. J. *Polymer* **1998**, *39*, 4541.
(3) Mathot, V. B. F.; Scherrenberg, R. L.; Pijpers, T. F. J.; Bras, W. *J. Therm. Anal.* **1998**, *46*, 681.
(4) Mathot, V. B. F.; Pijpers, M. F. J. *J. Appl. Polym. Sci.* **1990**, *39*, 979.
(5) Minick, J.; Moet, A.; Hiltner, A.; Baer, E.; Chum, S. P. *J. Appl. Polym. Sci.* **1995**, *58*, 1371.
(6) Androsch, R. *Polymer* **1999**, *40*, 2805.
(7) Androsch, R.; Wunderlich, B. In *Proceedings of the 26th NATAS Conference*, Cleveland, OH, Sept 13−15, 1998; Williams, K. R., Ed.; 1998; Vol. 26, p 469.
(8) Gaur, U.; Wunderlich, B. *Macromolecules* **1980**, *13*, 445.
(9) Androsch, R.; Blackwell, J.; Chvalun, S. N.; Wunderlich, B. *Macromolecules* **1999**, *32*, 3735.
(10) Androsch, R.; Wunderlich, B.; Blackwell, J.; Chvalun, S. N. Presented at the APS Centennial Meeting March 20−26, Atlanta, GA; *Bull. Am. Phys. Soc.* **1999**, *44* (2), 1562.
(11) McFaddin, D. C.; Russell, K. E.; Wu, G.; Heyding, R. D. *J. Polym. Sci., Phys.* **1993**, *31*, 175.
(12) Bensason, S.; Minick, J.; Moet, A.; Chum, S. P.; Hiltner, A.; Baer, E. *J. Polym. Sci., Phys.* **1996**, *34*, 1301.
(13) Peeters, M.; Goderis, B.; Vonk, C.; Reynaers, H.; Mathot, V. *J. Polym. Sci., Phys.* **1997**, *35*, 2689.
(14) Wunderlich, B. *Macromolecular Physics*; Academic Press: New York, 1976; Vol. 2.
(15) Boller, A.; Jin, Y.; Wunderlich, B. *J. Therm. Anal.* **1994**, *42*, 307.
(16) Reading, M.; Hahn, B. K.; Crowe, B. S. U.S. Patent, Method and Apparatus for Modulated Differential Analysis, 5,224,775, July 6, 1993.
(17) Reading, M.; Luget, A.; Wilson, R. *Thermochim. Acta* **1994**, *138*, 295.
(18) Wunderlich, B. *J. Therm. Anal.* **1997**, *48*, 207.
(19) Wunderlich, B.; Boller, A.; Okazaki, I.; Ishikiriyama, K. *Thermochim. Acta* **1997**, *304/305*, 125.
(20) Androsch, R.; Moon, I.; Kreitmeier, S.; Wunderlich, B. *Thermochim. Acta*, in press.
(21) Androsch, R.; Wunderlich, B. *Thermochim. Acta* **1999**, *333*, 27.
(22) Wunderlich, B.; Boller, A.; Okazaki, I.; Ishikiriyama, K.; Chen, W.; Pyda, M.; Pak, J.; Moon, I.; Androsch, R. *Thermochim. Acta* **1999**, *330*, 21.
(23) Okazaki, I.; Wunderlich, B. *Macromolecules* **1997**, *30*, 1758; *Macromol. Chem. Phys., Rapid Commun.* **1997**, *18*, 313.
(24) Ishikiriyama, K.; Wunderlich, B. *Macromolecules* **1997**, *30*, 4126; *J. Polym. Sci., Part B: Polym. Phys.* **1997**, *35*, 1877.
(25) Schick, C.; Merzlyakov, M.; Wunderlich, B. *Polym. Bull.* **1998**, *40*, 297.
(26) Product Information, DuPontDow Elastomers, Wilmington, USA.
(27) Product Information, Dow Plastics, Midland, USA.
(28) Keating, M. Y.; Lee, I.-H. *J. Macromol. Sci., Phys.*, in press.
(29) Lai, S.; Plumley, T. A.; Butler, T. I.; Knight, G. W.; Kao, C. I. *Proc. SPE ANTEC* **1994**, 1814.
(30) Lai, S.; Wilson, J. R.; Knight, G. W.; Stevens, J. C.; Chum, P. W. US Patent 5,272,236 Dec 21, 1993.
(31) Wunderlich, B. *Thermal Analysis*; Academic Press: New York, 1990.
(32) Advanced THermal Analysis System: Wunderlich, B. *Pure Appl. Chem.* **1995**, *67*, 1919. For downloadable data use WWW (Internet): URL: http://web.utk.edu/~athas.
(33) Pyda, M.; Wunderlich, B. *Macromolecules* **1999**, *32*, 2044.
(34) Wunderlich, B.; Dole, M. *J. Polym. Sci.* **1957**, *24*, 201.
(35) Wunderlich, B. *Macromolecular Physics*; Academic Press: New York, 1980; Vol. 3.
(36) Fu, Q.; Chiu, F.; McCreight, K. W.; Guo, M.; Tseng, W. W.; Cheng, S. Z. D.; Keating, M. Y.; Hsieh, E. T.; DesLauries, P. J. *J. Macromol. Sci., Phys.* **1997**, *B36* (1), 41.
(37) Wunderlich, B.; Sullivan, P.; Arakawa, T.; DiCyan, A. B.; Flood, J. F. *J. Polym. Sci., Part A* **1963**, *1*, 3581.
(38) Schawe, J. E. K.; Bergmann, E. *Thermochim. Acta* **1997**, *304/305*, 179.
(39) Schawe, J. E. K. *J. Polym. Sci., Phys.* **1998**, *36*, 2165.
(40) Toda, A.; Oda, T.; Hikosaka, M.; Saruyama, Y. *Thermochim. Acta* **1997,** *293*, 47.
(41) Toda, A.; Tomita, C.; Hikosaka, M.; Saruyama, Y. *Polymer* **1998**, *39*, 5093.
(42) Magonov, S., unpublished data by atomic force microscopy (AFM).
(43) Wunderlich, B. *Macromolecular Physics*; Academic Press: New York, 1973; Vol. 1.
(44) Ishikiriyama, K.; Boller, A.; Wunderlich, B. *J. Therm. Anal.* **1997**, *50*, 547.
(45) Mehta, A.; Wunderlich, B. *Makromol. Chem.* **1972**, *153*, 327; *Colloid Polym. Sci.* **1975**, *253*, 193. Wunderlich, B. *Discuss. Faraday Soc.* **1979**, *68*, 239.
(46) Albrecht, T.; Strobl, G. *Macromolecules* **1995**, *28*, 5827.
(47) Strobl, G. R.; Schneider, M. J.; Voigt-Martin, G. *J. Polym. Sci., Phys.* **1980**, *18*, 1361.
(48) Schultz, J. M.; Fischer, E. W.; Zachmann, H. A. *J. Polym. Sci., Phys.* **1980**, *18*, 239.
(49) Wunderlich, B.; Baur, H. *Fortschr. Hochpolym.-Forsch.* (*Adv. Polym. Sci.*) **1970**, *7*, 151.
(50) Sumpter, B. G.; Noid, D. W.; Liang, G. L.; Wunderlich, B. *Adv. Polym. Sci.* **1994**, *116*, 27; see also *J. Phys. Chem.* **1994**, *98*, 11739.
(51) Pyda, M.; Boller, A.; Grebowicz, J.; Chuah, H.; Lebedev, B. V.; Wunderlich, B. *J. Polym. Sci., Part B: Polym. Phys.* **1998**, *36*, 2499; and submitted.
(52) Ishikiriyama, K.; Pyda, M.; Zhang, G.; Forschner, T.; Grebowicz, J.; Wunderlich, B. *J. Macromol. Sci., Phys.* **1998**, *B37*, 27.

MA9905223